

A quantitative and comparative study of sputtering yields in Au

J. Samela* J. Kotakoski K. Nordlund J. Keinonen

Accelerator Laboratory, P.O. Box 43, FIN-00014 University of Helsinki, Finland

Abstract

We have systematically tested two entirely independent, empirical potentials (EAM and MD/MC CEM) which are widely used in classical molecular dynamics simulations by simulating Xe ion impacts to the Au(111) surface in the broad energy range between 0.1 – 200 keV. Special attention is paid to ensure that the simulated results are statistically significant. We have also compared simulations to experimental results on sputtering yields and crater production. Both potentials bring about qualitatively similar outcomes of the collision cascades, giving good confidence that the previous conclusions drawn from simulations on heat spike behaviour in dense metals are valid. However, the quantitative results are different. The MD/MC CEM potential has clearly better agreement with experimental sputtering yield data than the EAM potential, although neither potential agrees with experiments in the full energy range studied.

Key words: interatomic potential, sputtering, collision cascade, molecular dynamics, ion irradiation, heat spikes, cratering

PACS: 79.20.Ap, 34.20.Cf, 79.20.Rf, 34.50.Dy

1 Introduction

Heavy ion bombardment of heavy metals at keV energies is a prototype of ion irradiations where heat spikes are important for the outcome of collision cascades. The topic has been studied much by both experiments and computer simulations, giving a good qualitative picture of what happens. However, few studies have attempted to test whether it is possible to obtain quantitative

* Corresponding author.

Email address: juha.samela@helsinki.fi (J. Samela).

agreement between theory and experiment, which would give good confidence that the qualitative conclusions drawn from simulations are reliable.

Brinkman proposed in 1954 that an energetic ion in a dense material may not only displace a few isolated atoms, but in fact for a brief time produces entirely empty regions surrounded by a highly overdense one [1]. Ever since then the precise nature and even the existence of such heat spikes, also called collisional spikes or thermal spikes, has been subject to debate. The very high temperature (thousands of Kelvins) and short time scale (a few picoseconds) associated with the heat spikes make them an entirely non-equilibrium phenomenon. Hence it was not clear for a long time whether ordinary thermodynamic concepts can be used at all in describing the spikes. Also the most common tool to simulate irradiation effects, the binary collision approximation [2], is not suitable to simulate heat spikes since it breaks down when the recoil energies approach thermal energies. It was only in the 1980's when computer capacity advances made it possible to simulate collision cascades using molecular dynamics [3–5] that a certainty of the nature of heat spikes started to emerge. By now it is clear that heat spikes do exist and in fact resemble surprisingly much the original prediction of Brinkman [6].

Two of the main evidences of heat spikes are related to surface effects of ion irradiation. Sputtering yields have been observed to increase non-linearly with energy when heavy ions bombard heavy metals [7–11]. Also the surface morphology changes due to irradiation, especially the formation of craters and even more exotic structures [12–15], is hard to explain with any other mechanism than the liquid flow from heat spikes [16,17].

Molecular dynamics (MD) simulations have been invaluable in giving understanding of sputtering and crater formation from heat spikes [18,16,17,19–23]. Most of the studies to date have, understandably, focussed on obtaining qualitative understanding of the atom displacement mechanisms, employed a single atomic interaction model, and considered only a few ion energies. It would, however, be very useful to know how reliable the models are quantitatively, and whether agreement with experiments in a narrow energy range implies that the model used is reliable in a wider one. The cluster emission study by Colla et al. [19] is an example of quantitative comparison of simulations to experimental results.

In this work we address these questions by simulating Xe ion impacts on Au(111) surfaces at ion energies varying from 0.1 to 200 keV, i.e. more than 3 orders of magnitude. We chose this particular system because there is good experimental data available on both the sputtering yield [24] and crater formation [14,15]. We also simulate Ar impacts at energies 1-5 keV, another case where good experimental data on sputtering from a single-crystalline Au(111) surface is available. We employ two different interatomic potentials, the EAM

[25] and MD/MC CEM [26] ones. Both are conceptually based on the effective medium theory but are otherwise very different in the approach to their derivation. Hence comparing results obtained with the two potentials provides a good test base on how sensitive the qualitative and quantitative sputtering yield results are to the potential choice. In addition to the EAM and CEM models used in this work, there are numerous other many-body potential schemes for metals (see e.g. [27,28,85,30,31] and references therein).

We pay special attention to get statistically reliable values for simulated sputtering yields and other quantities. The experimental sputtering yield is an average of numerous sputtering events. To be able to compare experimental and simulated yields, the series of simulation runs should be long enough to prevent an individual run to change considerably average yield or other physically interesting values. Especially at high energies, the yield can vary from zero to several thousand atoms per ion between individual simulated events. If the simulation series is too short, the average yield can for instance double after adding a single new event in the series.

2 Methods

2.1 Overview of potentials

The interatomic potentials based on the effective medium theory (EMT) are and will be a very important practical tool for large scale MD simulations, and thus the knowledge of their proper application areas are of great importance. In spite of the drawbacks, the potentials provide very encouraging results, which is also demonstrated in the present study.

The drawbacks of potentials based on the EMT are well known and have two different sources [32]. First, the EMT is based on approximations, which are insufficient in many situations. Second, the development of potentials is sometimes based on a too small database of experimental values and too few fitting parameters resulting in potentials, which could be better within the intrinsic limitations of the EMT. This is not a drawback of the EMT method itself. In addition to these facts, the present study demonstrates that different EMT implementations, which are originally developed to simulated equilibrium properties of metals, can give very different results when applied to nonequilibrium phenomena like sputtering.

The embedded atom method (EAM) is based on the effective medium theory and was developed in 1983 by Daw and Baskes for calculations of ground state properties of realistic metal systems [33,34]. It is widely used and gives

a good agreement to experimental values of basic properties of bulk metals ([35] and references therein). For example, the lattice constant and the bulk modulus are reproduced exactly since the potential function was fitted to reproduce these properties. Foiles concluded that the EAM formalism is capable of providing a good description also for the liquid state [36]. Therefore it is applicable to simulations of systems where the solid and liquid phases co-exist, like in ion impacts to metals. However, it soon became clear that although the EAM potentials are valid for bulk metals and also fairly good for sputtering simulations, the functionals should be modified to get a better agreement with experimental sputtering data [37]. The EAM potential for Au is fitted to empirical data by Foiles et al. [35].

In 1988 DePristo and co-workers developed an corrected effective medium theory (CEM) [38] and later an approximation of it, which is better suitable for large scale MD simulations and gives good agreement with experimental data in many respects, for example in metal surface relaxations [39–42]. The latter method is termed “molecular dynamics and Monte Carlo corrected effective medium” (MD/MC-CEM) and it is abbreviated as CEM in the present study. Previous works have shown, that this potential describes better sputtering phenomena than the EAM potential in some metals. Wucher and Garrison reported that the CEM potential describes better the Ag clusters emitted as a part of sputtering flux from Ag surfaces [43]. The angular dependence of sputtering yields from Ni and Rh targets is found to agree better with experimental values when CEM is used instead of EAM [44].

The CEM potentials differ from the EAM potentials in one important respect relevant to the current work ([44] and references therein). The CEM functional is fitted to bulk properties, as well as to *ab initio* dimer data, whereas the EAM functional is fitted only to the bulk properties.

The CEM potential is also applicable to study surface phenomena. It reproduces reasonably well the surface energy of Au [45]. Udler and Seidman found that the CEM and EAM provide different values for surface energies of different lattice surfaces in several metals [46]. We have obtained that for Au the simulated surface energy with the CEM potential is $1.4 J/m^2$ and it is $0.8 J/m^2$ with the EAM potential [47]. The experimental value of surface energy is difficult to determine, but a recent study [48] indicates that $1.51 J/m^2$ is a good value. Thus, the CEM potential is likely to be better for simulations of surface phenomena.

Melting temperatures for the potentials have also been determined in an earlier study in our group [47]. The results are 1635 ± 5 K for CEM and 1110 ± 20 K for EAM. The empirical melting temperature for Au is 1337 K [49].

As far as we know, there are no comparisons of the potentials to experimen-

tal sputtering yield data in Au covering the energies between 0.1-200 keV. However, there are comparisons with other elements which clearly indicate that results calculated with the CEM potential are closer to experimental results than those calculated with the EAM potential and with other potentials. Colla et al. [19] have studied Ar impacts onto Cu(111) and found that dimer fraction of sputtering yield calculated with the CEM potential is closer to experimental value than with the other potentials in the comparison although the simulated value is still a factor of 4 larger than experimental results. Rosencrance et al. [50] have measured angular distributions of Ni and Rh atoms desorbed by Ar ion bombardment. They found that the CEM potential improves the agreement with experimental data compared to the EAM potential.

2.2 Simulation of irradiation events

The molecular dynamics simulation principles have been described in detail elsewhere [51–53,20], so here we only summarise the features which are essential for the potential comparison.

The Au-Au interactions are described in the simulations with the EAM and CEM potentials described above. At small interatomic distances both potentials were smoothly joined to the universal repulsive potential. The particular versions of potentials used in this study and the main differences between them are discussed in ref. [47].

Electronic stopping was applied as a non-local frictional force to all atoms having a kinetic energy larger than 5 eV [54,55]. Since ion channeling is not particularly important for the sputtering or crater formation considered in this paper, and even the stopping in channels is dominated by the nuclear stopping part under the irradiation conditions considered in this paper, we did not consider it necessary to use a local stopping model [56] in the current work.

We used the same simulation software and the same values of parameters with both potentials whenever applicable. The following process was repeated for both potentials and different sizes of simulation cells. First, the initial simulation cells were heated up from 0 K to 100 K with periodic boundary conditions in all directions to get the proper lattice constants for the simulation temperature. After that, one surface was opened and relaxed for 20–30 ps to reach equilibrium conditions before the ion impact. The relaxation did not change the crystal structure in the surface region, except for the small inwards relaxation of the outermost atom layer. Therefore the simulations describe how the collision cascades evolve in perfect lattice. The Xe-Au and Ar-Au

Table 1

Affect of temperature control time constant to sputtering yields (atoms/ion). Average yields of 10 simulations at 5 keV.

Time constant	EAM	CEM
20 fs	17.1 ± 3.5	17.1 ± 2.4
200 fs	16.6 ± 3.3	17.1 ± 2.4
2000 fs	16.3 ± 3.2	17.1 ± 2.4

interactions were described with a pair potential calculated using the DMOL software [57–59].

Simulations were carried out for a Au(111) surface and the ions were targeted perpendicular to the surface corresponding to the experimental condition. The impact point on the surface was chosen randomly within an area of one unit cell and stratified sampling was used to ensure uniform distribution of impact points within that area [60]. More precisely, the unit cell area is divided into nine subcells of equal size and impact points are chosen randomly inside the subcells. Nine simulations thus cover the unit cell area more uniformly than simulations based on points chosen randomly within the total area of the unit cell. Stratified sampling decreases the error of the average yield when it is possible to run only a very limited number of simulations [60,61]. The simulation cell had periodic boundaries in the x and y dimension, open top layer in the +z direction, and fixed bottom layer in the -z direction. All events are simulated at an ambient temperature of 100 K.

The smallest simulation cell of 20 160 atoms was used for 100 eV events and the largest cell of 3 354 120 atoms for 100-200 keV CEM events. The sizes of the simulation cells were chosen to be large enough to prevent cascades to reach the cell boundaries and shock waves bouncing back from the opposite side of the simulation cell to disturb the cascade.

Berendsen temperature control was used to cool the sides and the bottom of the simulation cell to 100 K. The temperature scaling at the boundaries absorbed most of the shock wave emanating from the collision cascade. The thickness of cooling region was variable but always more than 6 Å. The time constant for the cooling was optimized to provide efficient cooling of the cell. We made several test runs at each energy to ensure that simulation lattice was large enough so that the fraction of the shock waves coming back due to the periodic boundary conditions do not affect collision cascade and heat was absorbed fast enough in the boundary layers. Table I shows results of comparison of sputtering yields observed using different time constants in temperature control. Shorter time constant means more rapid cooling. The sputtering yields are almost independent of cooling rate at 5 keV which indicates that the simulation cell is large enough for sputtering simulations.

We also used a trigger in our software to alarm if energetic recoil reaches to boundary and will come back from the other side. The simulation was stopped if this occurred. However, range calculations [62] showed that the ion range could be as large as 800 nm at 100 keV when channelling occurs. Therefore, in the energies between 50-200 keV we let Xe ions exit through the bottom of the simulation cell, which was located more than 35 nm from the surface. Visual inspection of simulation results showed that recoils and subcascades in 10 nm bottom layer of the simulation cell had no noticeable effect on spikes in upper layers, which are origins of sputtering and cratering. A simulation cell of at least 10 million atoms would be required to simulate events completely at 100 keV.

Shock waves are a well known problem in ion bombardment simulations. Because of the limited size of the simulation cell shock waves are reflected back from cell boundaries and the reflected wave can affect the collision cascade. Fixed boundaries reflect shock wave straight back to collision cascade region. If periodic boundary conditions are used, reflected waves come back from the opposite side of the cell. If boundaries are open, waves reflect back from boundary regions and, in addition, an energetic shock wave can also deform the target shape and even cause sputtering from open side boundaries.

Due to the chaotic nature of collision cascade it is always possible that even very weak reflected wave can cause remarkable change in collision cascade development. However, if statistics is collected from series of simulation runs, it is in practice possible to use an impact target which is large enough to avoid unrealistic effects caused by boundaries conditions at low energies. To simulate energetic events, this is not possible because target size should be unpractically large, e.g. tens of millions of atoms. In these cases a damping mechanism should be used.

Several strategies and mechanisms to damp shock waves are used in recent studies of ion or cluster impacts. Yamaguchi [63] applies a large target of more than one million atoms and a surrounding external region with velocity scaling and fixed outer boundary. Postawa et al. [64] uses generalized Langevin equation approach [65] to remove energy from boundary zones and fixed outer boundaries in C_60 impact simulations. This reduces sputtering 3-7 % compared to simulations with free boundaries. On opposite effect of free boundaries in Au ion bombardment to Au(111) target were found by Shapiro and Tombrello [66]. They found that sputtering yields were one-third to one-half of the yields observed experimentally if open boundary are used instead of their algorithm that reflects back part of the momentum from the bottom of the simulation cell. Colla et al. [67] have used rather large targets (240 000 atoms) and damping boundaries in Au sputtering simulations. Kornich et al. [68] have used periodic boundary conditions with an energy dissipation layer. Periodic boundary conditions and temperature control are also used by Hedstrm et al.

[69], Mazzone [70] and recently by Tucker et al. [71].

Bringa et al. have studied shock waves in simulation cell consisting of crystalline Cu using the EAM potential and periodic boundary conditions [72]. When pressure is above a certain value, two shock fronts are produced. The first is elastic wave which could produce few point defects. The second is plastic front moving faster than the elastic front and overtaking it. The plastic front may cause stacking faults as it travels through the pristine lattice. The crystal can even melt in the front of plastic waves.

This was observed also in our simulations and therefore we chose the simulation cells to be large enough to prevent plastic waves to reach boundaries before they are damped to elastic waves. In addition to this, we used temperature control based on velocity scaling in five sides of the simulation cells to damp elastic waves. When the width and depth of the simulation cell are doubled, the volume of damper zones becomes four times larger. Thus the damping volume was considerably larger at high ion energies because larger cells were used. Damped elastic waves reflected through periodic boundaries to opposite side of cell and back from the fixed bottom layer, but did not affect collision cascade in any noticeable way.

Because the intention was to simulate collisions to bulk crystal surface, periodic boundary conditions were used to prevent the surface atomic layers to move towards center of crater. If open boundaries are used, the upper layer moves one atomic position towards to the center and the surface is bend as a cupola, which is not expected to happen in surface of bulk crystal. Due to this, the sputtering yields of high yield events are lower when open boundaries were used.

2.3 Analysis

The experimental sputtering yield is an average of numerous sputtering events. In simulations, especially at high energies, the yield can vary from zero to several thousand atoms per ion between individual events. A single large yield event can increase the average yield significantly and the results are very sensitive to whether a single event is included in an average or not. To compare simulated results to experimental values it is necessary to run enough simulations with different random initial values. The results of this sensitivity analysis are shown in Fig. 1. About 40 simulations are required to stabilize the average yield at 500 eV and at high energies even twice as many simulations are required. In this study each simulation series at the energies between 0.1-5 keV included 99 runs and the average values can be considered reliable. At energies between 7 and 30 keV 45 simulations at each energy were enough to

give reliable averages. At higher energies the simulation series at each energy and with different potentials included 35-45 runs. Sensitivity analysis indicated that 50 and 100 keV average yields are quite reliable, but at 200 keV the standard error of the average underestimates the uncertainty.

Simulation times were chosen to be long enough to ensure that the probability of additional sputtering is very low. The prerequisite for this is, that the heat spike is cooled enough and stable conditions are reached in the 15 nm deep surface layer of the simulation cell. The high energy EAM events required the longest simulation times of up to 80 ps. The high energy CEM events, instead, were simulated only for 4 ps, because at these energies ions are usually penetrated deep into the lattice and the surface layers are cooled rapidly, usually in less than 2 ps. There could exist strong heat spikes 15-30 nm below the surface, but there is no indication, that it would cause sputtering, even if the simulation time would be longer.

The sputtering yields are calculated from the final states of the simulations. An atom or an atom cluster is considered sputtered, if it has no neighbour atoms nearer than 0.555 nm, which is the cutoff distance of the potentials, or a cluster of atoms is more than 0.555 nm away from the surface. Sputtering yields are also calculated during the simulation at specified times, but the time series of yields are analyzed only qualitatively.

The crater dimensions are calculated after the simulations using the following methods. The empty volume is calculated considering a rectangular volume of the simulation cell around and below the impact point. The volume is divided into small subcells, which have a volume of one cubic Ångström. A subcell is considered occupied, if it contains an atom or there is an atom in one of its neighbouring subcells. The volumes of the unoccupied subcells are summed up to get the total empty volume. This volume is the sum of the volumes of the main crater and vacancies in the neighbourhood and below the crater. Although it is not an exact measure of the crater volume, it is a reasonable measure to compare crater sizes and empty volumes caused by the two potentials. If a crater exists, the empty volume calculated comes mainly from the crater volume. If there is no crater, the empty volume is small and comes mainly from vacancies scattered below the impact point (although few 1 Å³ cubes will also be empty even in a perfect lattice when they happen to fall right in between the lattice planes). The crater depth is defined as the depth where the empty volume is for the first time less than a specified value, which is chosen to be 20 Å³. With this value bottoms of craters are detected reasonably well in this analysis. We measured dimensions of some craters also manually from the visualizations of the simulations to ensure the correctness of the analysis. The empty volume 0.3 nm below the lattice surface is considered to give the crater area. This depth is chosen to exclude surface defects from contributing to the area calculation.

In addition, the crater rim diameters were measured by scanning the surface of the simulation cell along two perpendicular directions and by detecting the first and the last point where atoms are stacked onto the surface. Because the crater rims are very irregular, this method, like any other method to measure rim diameters, is only approximative.

Crater shapes and defects are qualitatively analyzed from visualizations of simulation results and profiles of empty volumes (e.g. Fig. 6).

Relations between sputtering yield and crater dimensions are analysed by calculating correlation coefficients, which are measures of linear association between two variables [60]. Zero value indicates no linear association. The closer the value is to +1 or -1 the more closely the two variables are related.

3 Results

3.1 Sputtering yield

Comparison of experimental [24] and simulated sputtering yields is shown in Fig. 2.

Both potentials give too high yields at ion energies below 1 keV. Analysis of simulations gives no obvious explanation for this disagreement. One reason might be the differences between simulated and real lattice surfaces, because at these energies collision leading to sputtering occur very near the lattice surface. In simulations the surface is perfect whereas in reality there is some roughness and the surface orientation might vary. However, at energies below 1 keV both potentials give good qualitative agreement for the sputtering yield as a function of the energy, although we observed differences in collision mechanisms, as will be shown below.

The agreement between simulated and measured yields is good at energies between 1 and 3 keV. At the energies higher than 5 keV the EAM yields are several times higher than the experimental yields.

At high energies the portion of zero yield cases increases rapidly, because ions penetrate deep into the lattice and almost no surface cascades appear in these cases. This can be observed with both potentials, but the increase of zero events is more notable in the CEM events. There are almost no high yield events in the 200 keV CEM simulation series. Therefore, at energies of 200 keV and higher the CEM simulations give too low yields. The simulation serie is statistically long enough to exclude the possibility, that this disagreement

arises by chance.

Simulations with the EAM potential at 400 keV show that the yield is indeed decreasing when energy increases, the simulated average yield being 79 ± 47 atoms/ion at 400 keV. There is no experimental value available for comparison, but extrapolation of the 200–300 keV results give an estimate of not more than 50 atoms/ion. Thus, the EAM yield is still too high at 400 keV.

Both potentials result in the same qualitative forms of yield distributions at different energies, as shown in Fig. 3. However, the portion of high yield events increases more rapidly with energy in the EAM simulations than in CEM simulations. At 100 eV and 1 keV all events have low yield and the distributions are very similar. Notice that at least one atom is sputtered in nearly every 1 keV event. At 5 keV the distribution is spread and the difference between potentials becomes visible. At 20 keV there are more high yield EAM events than CEM events, while most of the CEM cases have yields between 5-30 atoms/ion. The same is true at 100 keV. Thus the difference between the CEM and EAM yields is mainly due to the greater portion of high yield events in the EAM simulations. The conclusion is, that simulations with the EAM potential bring about unrealistically many high yield events.

There is also a qualitative difference between potentials regarding the high yield events. In the CEM events almost no sputtering occurs after 10 ps, whereas in the EAM events atoms or even atom clusters are emitted from the surface of crater rims during a much longer period. The CEM potential seems to bind the atoms in craters and in crater rims more tightly than the EAM potential. However, the potentials give the same qualitative behaviour, that most of the sputtering occurs during about 2 ps after the impact and the fastest sputtered atoms leave the surface.

In addition to individual Au atoms, also atom clusters of different sizes are sputtered from the target. The simulated cluster sputtering yield is 0.11 ± 0.08 clusters/ion for CEM and 1.0 ± 0.35 for EAM at 50 keV, when clusters containing over ten atoms are considered. Thus ten times more clusters are ejected in the EAM simulations than in the CEM simulations. Wucher and Garrison [43] have made the same observation and found that the CEM potential provides an almost quantitative description of the experimental cluster yields. According to them the EAM potential overbinds clusters.

For comparison we also simulated some argon to gold impacts at energies 1-5 keV (Fig. 4). The results are in good agreement with the experimental data [73,74], although the EAM events have slightly higher sputtering yields than the CEM events.

3.2 Crater formation

In the simulations, craters of different sizes and shapes can be seen in the lattices. However, the percentage of cratering events is different depending on the potential used in the simulation (Fig. 5). In the EAM simulations, there appears considerably more craters than in the CEM simulations at all energies up to 50 keV.

Donnelly and Birtcher [75] have measured cratering of gold when irradiated with Xe ions using transmission electronic microscopy (TEM). They observed that approximately 2-5% of impinging ions in the energy range 50-400 keV produce craters. This is about five times less than we observed in the simulations (Fig. 5). The likely explanation to this disagreement is, that also quite small craters are easily observed in simulation results, which increases the total amount of crater events. The smallest craters may either not be visible in the TEM experiments (note that in these experiments a large underfocus was used so they can not achieve atomic resolution), or may be thermally annihilated before observation [76]. The large craters, however, are experimentally known to be stable at room temperature [77,76]. On the other hand, we observed only a few large craters in the 100 keV and 200 keV CEM series, so the production rate of large craters in the CEM simulations is less than 10 %, whereas in the corresponding EAM series, the large crater rate is higher than 10 %. From these observations, it follows that the EAM potential probably forms too many craters compared to the experimental cratering rate at the energies 100-200 keV, whereas the CEM potential produces almost the right cratering rate.

At 1 keV one third of the EAM events form craters, whereas in the CEM events only depressed areas and additional atoms above the lattice surface can be seen. This leads to the conclusion that at energies between 1-5 keV the heat spikes and thus also the sputtering mechanism are different depending on the potential applied in spite of the fact, that the sputtering yield is almost the same and agrees well with the experimental yield.

The EAM heat spikes grow larger than the spike of the CEM events and their sputtering lasts longer. On the other hand, the phases of spike formation are the same.

The difference in the shapes of craters can be seen also at high energies (Fig. 6). EAM craters are wider and there is often a larger rim around the crater. It is formed by atoms and clusters, which do not have enough energy to sputter out of the surface. In both cases there are vacancies below the craters.

The formation mechanism of large craters and comparison of the EAM crater simulations to experimental results are presented in more detail in earlier

papers by us [78,79]. We observed that during crater formation time of 100 ps some exotic structures like atom bridges over craters occur in simulations. Transmission electron microscope (TEM) experiments have also shown the formation of these and other, even more exotic structures on the irradiated surfaces [75]. This is an evidence, that the morphology of the simulated large EAM craters is qualitatively correct. We observed similar structures in this study in both EAM and CEM simulations. However, the structures were more common and more remarkable with the EAM potential.

3.3 Correlation between sputtering and cratering

Dimensions of craters as functions of ion energy are shown in the figures 8–10. The lower panels show the correlation between the quantity and sputtering yield. Positive correlation values indicate linear dependency. However, the dependency should be considered negligible if the correlation is less than 0.5.

The average crater area is larger in the EAM events than in the CEM events (Fig. 7). In both cases there is a positive correlation between sputtering yield and crater area, especially at the high ion energies. The correlation is about the same with both potentials. This confirms the conclusion, that the EAM heat spikes and craters grow larger than the CEM spikes, and more atoms are sputtered due to the larger cross section of liquid volume and lattice surface in the EAM events. Thus, the reason to the difference in sputtering yields between the potentials is not the mechanism how the atoms leave the liquid surface but rather the size of the heat spike, which, in turn, depends on how the potentials describe interactions on the atomic level in that part of the lattice, where the ion energy is rapidly deposited into a relatively small volume.

Also the average crater depth and the average empty volume are higher with the EAM events than with CEM events. Correlations with the yield are also positive (Fig. 8 and Fig. 9).

Average maximum outer diameter of crater rims increases linearly with ion energy (Fig. 10) when only events with visible craters are included in the analysis. It should be noted that rims are very irregular and therefore diameters are difficult to measure. However, the general trend towards larger craters as energy increases is clearly detectable.

In general, the crater dimensions correlate better with the sputtering yield when energy increases. This is a consequence of the fact, that at high energies the events are either very low or very high yield events as shown in the distribution graphs in Fig. 3 and the high yield events are also large crater events. We can say that most of the sputtered clusters and atoms come from large craters at energies of 100 keV and higher.

Table 2

Comparison of simulated (CEM and EAM) and measured crater areas in gold. The areas are given in units of nm^2 .

E (keV)	CEM	EAM	Exp.
50	16 ± 3	26 ± 5	14
100	15 ± 4	37 ± 9	-
200	6 ± 2	46 ± 14	32

Comparison between the simulated and measured [75] mean areas (nm^2) of large craters is given in Table 2. Note that the simulated areas are averages of crater areas of the large craters whereas Fig. 7 represents the averages of all craters. The large craters are those with clearly visibly crater shape and rim.

The result given in the Table II confirm that EAM craters are larger than CEM craters and probably also too large compared with real craters. The CEM craters are too small at 200 keV, which is in agreement with the observation that also the simulated yield is too small at that energy. This is a further evidence, that the simulations were not able to produce enough heat spikes near the lattice surface, which leads to the too low average sputtering yield.

This crater analysis shows, that the CEM and EAM potentials give different crater sizes, shapes and crater event percentage. The CEM simulations seem to be more realistic when we compare the results to the experimental results available. More precise comparison would require experimental values for crater dimensions measured from events of different ion energies.

3.4 Defects

In addition to craters, ion impacts also form defects inside the lattice. Visual analysis of the simulation lattices after the simulations revealed differences in defect formation between the potentials. The observations can be summarized as follows:

- Vacancies are formed near and below craters. There are more vacancies in EAM events than in CEM events and they are spread over a larger volume around the ion track.
- If the ion penetrates deep into the lattice, there are clusters of vacancies or even volume defects in the depth, where the main energy deposition has occurred. This phenomenon is more prominent with EAM.
- The lattice around the ion track may be shifted away from its equilibrium position along lattice planes perpendicular to the (111) plane. This coherent displacement has a triangular cross-section since the displacement occurs along the slip system of the fcc crystal [20], see Fig. 8. There are often rows

of vacancies along the triangle sides. Similar defects are observed in earlier simulations at the lattice surface [20], and now we observed them also inside the lattice. This phenomenon occurs more often at energies over 30 keV and with the CEM potential. The EAM potential seems to form more irregular defects.

Fig. 12 illustrates examples of CEM and EAM events, which have the typical differences described above. Neither of these events has a crater on the lattice surface. Instead, they show a clear and regular shift of atoms towards the surface, resulting from coherent displacement. Also inside there are clear dislocated regions of the crystal. In the simulations with the CEM potential almost all defects are in dislocated regions, and a top-view of this CEM event showed a clear triangular cross section of one of the dislocated regions, indicating that the structure is a (perfect or imperfect) stacking fault tetrahedron [80–82]. In the EAM event, on the other hand, a less regular defect structure is visible. On longer time scales, this complex defect structure would most likely reform into a more regular structure, even at low temperatures (note that the interstitial is mobile at very low temperatures, both in experiments and our simulation model [83–85]). Hence one can not directly compare this result to experiments and conclude which model would describe extended defect formation better. Nevertheless, the differences in defect formation provide an additional evidence, that the potentials cause different heat spike behaviour.

3.5 Back scattered Xe ions

Xe ions are scattered back from the lattice more often in the CEM events than in the EAM events (Fig. 11), especially at energies 100–500 eV. The difference in percentage of back scattered ions indicates, that the potentials do not bring about identical sputtering mechanisms even at low energies, although the sputtering yield is practically the same with the both potentials below 1 keV.

At high energies the ions penetrate deeper into the lattice in average and thus the percentage of back scattering events decrease with energy. Both potentials lead to this behaviour, and the quantitative difference between them is barely statistically significant.

4 Discussion and conclusions

We have shown that CEM and EAM potentials not only give different simulated sputtering yields, but also different heat spike behaviour and crater sizes.

This raises the question which potential is appropriate enough to be used in ion impact simulations. We can draw the following conclusions.

The main result is, that the agreement between simulated and experimental yield values depends not only on the potential chosen but also on ion energy. Our quantitative results on the sputtering yields can be treated in four energy regimes.

- At very lowest energies, $E < 500$ eV, both the EAM and CEM potentials overestimate the sputtering yield. This is likely to be due to some inadequacy in the description of the top surface layer, or that the potentials have not quite right values near the threshold displacement energy.
- Between 500 eV and 3 keV both potentials give good agreement with experimental sputtering yields. We also observe similarly good agreement for 1 - 5 keV Ar impacts. In this energy range the cascades are typical linear cascades, and heat spikes do not contribute to the sputtering yield. Since both models have been amended to have a realistic high-energy repulsive part, they should describe linear cascades correctly, which is reflected in the good agreement with experimental sputtering yields.
- Above 5 keV heat spike effects start to dominate the sputtering, and the potentials' different description of the thermodynamics of Au are reflected in the sputtering yield. The EAM potential strongly overestimates the sputtering yield, whereas CEM shows good agreement up to 100 keV.
- Finally, above 100 keV the both potentials result in a faster decrease of the sputtering yield than observed experimentally.

These observations clearly show that quantitative agreement with experimental values in one energy range does not guarantee that the potential is applicable to other energy ranges.

Since several thermodynamic properties of the material affect the heat spike behaviour, it is not possible to name a single material parameter which would explain the observed difference between EAM and CEM at energies 10 – 100 keV. The simulations show that the melting point and thermal conduction clearly affects the behaviour, since in CEM all sputtering ceases around 10 ps whereas in EAM late emission is observed up to 80 ps. The simulated melting point is about 500 K lower with EAM than with CEM, as mentioned above. We do, however, believe that another contributing factor is the too low surface energy of EAM: this makes it easy to form free surface, making it likely to sputter large chunks of matter.

The rapid decrease in the simulated yields above 100 keV is related to channeling, which apparently is not described in the simulations in a manner which exactly corresponds to the experiments. The simulations should be fairly reliable regarding channeling, since the high-energy repulsive interatomic po-

tentials are known to be accurate to at least within a few % [86,59], and the electronic stopping is not significant at these energies [86]. This is evidenced by recent MD range simulations which give very good agreement with experiments under channeling conditions especially when the nuclear stopping dominates [87,88,56]. Hence we raise the possibility that the cause of the discrepancy may be some difference between the simulated and experimental bombarding conditions. If in the experiments the beam was not perfectly aligned to the surface normal, or there was appreciable beam spreading, this could reduce the channeling, which in turn would shift the maximum in the sputter yield distribution to higher energies. If this is the case, the CEM potential may still be applicable at these energies, although it gave considerably too low yields in this study.

The other results like crater morphology, defects and the rate of back scattered ions indicate, that, in addition to the different sputtering yields, the potentials also bring about different sputtering mechanisms. The most immediate conclusion is that the CEM simulations are closer to the reality, because the agreement with sputtering yield is good in a broad energy range and, in contrast, the behaviour of heat spikes, like formation of large craters, in EAM simulations could be related to the unrealistically large sputtering yields. However, we can not precisely compare empty volume, back scattering rate and many other simulated results to experimental data. Therefore we can not claim for certain, how close the quantitative agreement between heat spikes in CEM simulations and the real heat spikes is. Further measurements and simulations would be needed to get answers to this question.

Although the quantitative results differ, the qualitative behaviour is in all main respects the same, giving good confidence that the previous conclusions drawn from simulations on heat spike behaviour in dense metals are valid.

Acknowledgements

We thank E. Salonen for critical comments on the manuscript. Generous grants of computer time from the Center for Scientific Computing in Espoo, Finland are gratefully acknowledged.

References

- [1] J. A. Brinkman, J. Appl. Phys. **25**, 961 (1954).
- [2] M. T. Robinson and I. M. Torrens, Phys. Rev. B **9**, 5008 (1974).

- [3] R. P. Webb and D. E. Harrison, Jr., Nucl. Instr. Meth. Phys. Res. **218**, 697 (1983).
- [4] R. P. Webb, D. E. Harrison, Jr., and K. M. Barfoot, Nucl. Instr. Meth. Phys. Res. B **7/8**, 143 (1985).
- [5] T. Diaz de la Rubia, R. S. Averback, R. Benedek, and W. E. King, Phys. Rev. Lett. **59**, 1930 (1987), see also erratum: Phys. Rev. Lett. **60** (1988) 76.
- [6] R. S. Averback and T. Diaz de la Rubia, in *Solid State Physics*, edited by H. Ehrenfest and F. Spaepen (Academic Press, New York, 1998), Vol. 51, pp. 281–402.
- [7] R. Behrisch (ed.), *Sputtering by Particle bombardment I* (Springer, Berlin, 1981).
- [8] H. H. Andersen and H. L. Bay, Radiation Effects **19**, 139 (1973).
- [9] H. H. Andersen and H. L. Bay, J. Appl. Phys. **45**, 953 (1974).
- [10] H. H. Andersen, A. Brunelle, S. Della-Negra, J. Depauw, D. Jacquet, Y. Le Beyec, J. Chaumont, and H. Bernas, Phys. Rev. Lett. **80**, 5433 (1998).
- [11] S. Bouneau, A. Brunelle, S. Della-Negra, J. Depauw, D. Jacquet, Y. L. Beyec, M. Pautrat, M. Fallavier, J. C. Poizat, and H. H. Andersen, Phys. Rev. B **65**, 144106 (2002).
- [12] K. L. Merkle and W. Jger, Phil. Mag. A **44**, 741 (1980).
- [13] W. Jäger and K. L. Merkle, Phil. Mag. A **57**, 479 (1988).
- [14] R. C. Birtcher and S. E. Donnelly, Phys. Rev. Lett. **77**, 4374 (1996).
- [15] S. E. Donnelly and R. C. Birtcher, Phys. Rev. B **56**, 13599 (1997).
- [16] M. Ghaly and R. S. Averback, Phys. Rev. Lett. **72**, 364 (1994).
- [17] M. Ghaly, K. Nordlund, and R. S. Averback, Phil. Mag. A **79**, 795 (1999).
- [18] H. M. Urbassek and K. T. Waldeer, Phys. Rev. Lett. **67**, 105 (1991).
- [19] Th. J. Colla, H. M. Urbassek, A. Wucher, C. Staudt, R. Heinrich, B. J. Garrison, C. Dandachi, and G. Betz, Nucl. Instr. Meth. Phys. Res. B **148**, 284 (1998)
- [20] K. Nordlund, J. Keinonen, M. Ghaly, and R. S. Averback, Nature **398**, 49 (1999).
- [21] T. J. Colla, R. Aderjan, R. Kissel, and H. M. Urbassek, Phys. Rev. B **62**, 8487 (2000).
- [22] R. Aderjan and H. M. Urbassek, Nucl. Instr. Meth. Phys. Res. B **164-165**, 697 (2000).
- [23] E. Bringa, K. Nordlund, and J. Keinonen, Phys. Rev. B **64**, 235426 (2001).

- [24] W. Szymczak and K. Wittmaack, Nucl. Instr. Meth. Phys. Res. B **82**, 220 (1993).
- [25] S. M. Foiles, M. I. Baskes, and M. S. Daw, Phys. Rev. B **33**, 7983 (1986), *Erratum: ibid*, Phys. Rev. B **37**, 10378 (1988).
- [26] C. L. Kelchner, D. M. Halstead, L. S. Perkins, N. M. Wallace, and A. E. DePristo, Surf. Sci. **310**, 425 (1994), and references therein.
- [27] David G. Pettifor, Bonding and Structure of Molecules and Solids (Oxford University Press, Oxford, UK, 1995).
- [28] R. Smith (ed.), Atomic & ion collisions in solids and at surfaces: theory, simulation and applications (Cambridge University Press, Cambridge, UK, 1997).
- [29] Murray S. Daw, Stephen M. Foiles and Micael I. Baskes, Mat. Sci. and Engr. Rep. **9**, 251 (1993).
- [30] D. W. Brenner, Physica Status Solidi (b) **207**, 23 (2000).
- [31] K. Albe, K. Nordlund and R. S. Averback, Phys. Rev. B **65**, 195124 (2002).
- [32] D. F. Y. Mishin, M. J. Mehl, and D. A. Papaconstantopoulo, Phys. Rev. B **59**, 3393 (1999).
- [33] M. S. Daw and M. I. Baskes, Phys. Rev. B **29**, 6443 (1984).
- [34] M. S. Daw and M. I. Baskes, Phys. Rev. Lett. **50**, 1285 (1983).
- [35] S. M. Foiles, M. I. Baskes, and M. S. Daw, Phys. Rev. B **33**, 7983 (1986), *Erratum: ibid*, Phys. Rev. B **37**, 10378 (1988).
- [36] S. M. Foiles, Phys. Rev. B **32**, 3409 (1985).
- [37] B. J. Garrison, N. Winograd, D. M. Deaven, C. T. Reimann, D. Y. Lo, T. A. Tombrello, D. E. Harrison, and M. H. Shapiro, Phys. Rev. B **37**, 7197 (1988).
- [38] J. D. Kress and A. E. DePristo, J. Chem. Phys **88**, 2596 (1988).
- [39] M. S. Stave, D. E. Sanders, T. J. Raeker, and A. E. DePristo, J. Chem. Phys. **90**, 4413 (1990).
- [40] T. J. Raeker and A. E. DePristo, Int. Rev. Phys. Chem. **10**, (1991).
- [41] S. B. Sinnott, M. S. Stave, T. J. Raeker, and A. E. DePristo, Phys. Rev. B **44**, 8927 (1991).
- [42] T. J. Raeker and A. E. DePristo, Phys. Rev. B **49**, 8663 (1994).
- [43] A. Wucher and B. J. Garrison, J. Chem. Phys. **105**, 5999 (1996).
- [44] S. W. Rosencrance, J. S. Burnham, D. E. Sanders, C. He, B. J. Garrison, N. Winograd, Z. Postawa, and A. E. DePristo, Phys. Rev. B **52**, 6006 (1995).

- [45] A. E. DePristo, in *Recent Advances in Density Functional Theory: Part 2 Methodology*, edited by D. Chong (World Scientific, New York, 1995).
- [46] D. Udler and D. N. Seidman, Phys. Rev. B **54**, 11133 (1996).
- [47] K. O. E. Henriksson, K. Nordlund, and J. Keinonen, Phys. Rev. B (2004), accepted for publication.
- [48] Q. Jiang, H. M. Lu, and M. Zhao, J. Phys.: Condens. Matter **16**, 521 (2004).
- [49] D. R. Lide, *CRC Handbook of Chemistry and Physics*, 82nd ed. ed. (CRC Press LLC, Boca Raton, FL, USA, 2001).
- [50] S. W. Rosencrance, J. S. Burnham, D. E. Sanders, C. He, B. J. Garrison, N. Winograd, Z. Postawa, and A. E. DePristo, Phys. Rev. B **52**, 6006 (1995).
- [51] M. Ghaly, K. Nordlund, and R. S. Averback, Phil. Mag. A **79**, 795 (1999).
- [52] K. Nordlund, M. Ghaly, R. S. Averback, M. Caturla, T. Diaz de la Rubia, and J. Tarus, Phys. Rev. B **57**, 7556 (1998).
- [53] K. Nordlund, L. Wei, Y. Zhong, and R. S. Averback, Phys. Rev. B (Rapid Comm.) **57**, 13965 (1998).
- [54] K. Nordlund, Comput. Mater. Sci. **3**, 448 (1995)
- [55] J. F. Ziegler, J. P. Biersack, and U. Littmark, *The stopping and range of ions matter* (Pergamon, New York, USA, 1985).
- [56] J. Sillanp, J. Peltola, K. Nordlund, J. Keinonen, and M. J. Puska, Phys. Rev. B **63**, 134113 (2000).
- [57] J. Delley, J. Chem. Phys. **92**, 508 (1990).
- [58] DMol is a trademark of AccelRys. Inc.
- [59] K. Nordlund, N. Runeberg, and D. Sundholm, Nucl. Instr. Meth. Phys. Res. B **132**, 45 (1997).
- [60] W. H. Press, s. A. Teukolsky, V. T. Vetterling, and B. P. Flannery, *Numerical Recipes in C: The Art of Scientific Computing*, 2nd ed. ed. (Cambridge University Press, New York, USA, 1993).
- [61] T. J. Colla, B. Briehl, and H. M. Urbassek, Radiation Effects and Defects in Solids **142**, 415 (1997).
- [62] K. Nordlund and A. Kuronen, Nucl. Instr. Meth. Phys. Res B. **115**, 528 (1995).
- [63] Y. Yamaguchi and Jrgen Gspann, Phys.Rev. B **66** (2002) 155408.
- [64] Z. Postawa et al., Anal. Chem. **75** (2003) 4402-4407.
- [65] B. J. Garrison, P. B. S. Kodali, and D. Srivastava, Chem. Rev. **96** (1996) 1327.
- [66] M. H. Shapiro and T. A. Tombrello, Surf. Sci. **453** (2000) 143-151.

- [67] T. J. Colla, R. Aderjan, R. Kissel and H. M. Urbassek, Phys. Rev. B **62**, 12 (2000) 8487-8493.
- [68] G. V. Kornich, G. Betz, V. Zaporozhchenko, A. I. Bazhin and F. Faupel, Nucl. Instr. Meth. Phys. Res. B **227** (2005) 261-270.
- [69] M. Hedström and Hai-Ping Cheng, Phys. Rev. B **62** (2000) 2751-2758.
- [70] A. M. Mazzone, J. Computer-Aided Mat. Design **9** (2002) 1-9.
- [71] O. J. Tucker, D. S. Ivanov, L. V. Zhigilei, R. E. Johnson and E. M. Bringa, Nucl. Instr. Meth. Phys. Res. B **228** (2005) 163-169.
- [72] E. M. Bringa, B. D. Wirth, M. J. Caturla, J. Stlken and D. Kalantar, Nucl. Instr. Meth. Phys. Res. B **202** (2002) 56-63.
- [73] A. L. Southern, W. R. Willis, and M. T. Robinson, J. Appl. Phys **34**, 153 (1963).
- [74] M. T. Robinson and A. L. Southern, J. Appl. Phys **38**, 2969 (1967).
- [75] S. E. Donnelly and R. C. Birtcher, Phys. Rev. B **56**, 13599 (1997).
- [76] S. E. Donnelly, R. C. Birtcher, and K. Nordlund, in *Engineering Thin Films and Nanostructures with Ion Beams*, edited by E. J. Knystautas (Marcel Dekker, New York, 2005), Chap. Single Ion Induced Spike Effects on Thin Metal Films: Observation and Simulation.
- [77] R. C. Birtcher and S. E. Donnelly, Materials Chemistry and Physics **54**, 111 (1998).
- [78] K. Nordlund, J. Tarus, J. Keinonen, S. Donnelly, and R. Birtcher, Nucl. Instr. Meth. Phys. Res. B **206**, 189 (2003).
- [79] E. M. Bringa, K. Nordlund, and J. Keinonen, Phys. Rev. B **64**, 235426 (2001).
- [80] J. Silcox and P. B. Hirsch, Phil. Mag. **4**, 72 (1959).
- [81] M. Kiritani, T. Yoshiie, and S. Kojima, J. Nucl. Mater. **141-143**, 625 (1986).
- [82] K. Nordlund and F. Gao, Appl. Phys. Lett. **74**, 2720 (1999).
- [83] R. C. Birtcher, W. Hertz, G. Fritsch, and J. E. Watson, Proc. Intl. Conf. on Fundamental Aspects of Radiation Damage in Metals, CONF-751006-P1, **1**, 405 (1975).
- [84] H. Schroeder and B. Stritzker, Radiation effects **33**, 125 (1977).
- [85] M. S. Daw, S. M. Foiles, and M. I. Baskes, Mat. Sci. and Engr. Rep. **9**, 251 (1993).
- [86] J. F. Ziegler, J. P. Biersack, and U. Littmark, *The Stopping and Range of Ions in Matter* (Pergamon, New York, 1985).
- [87] D. Cai, N. Grnbech-Jensen, C. M. Snell, and K. M. Beardmore, Phys. Rev. B **54**, 17147 (1996).
- [88] J. Sillanp, K. Nordlund, and J. Keinonen, Phys. Rev. B **62**, 3109 (2000).

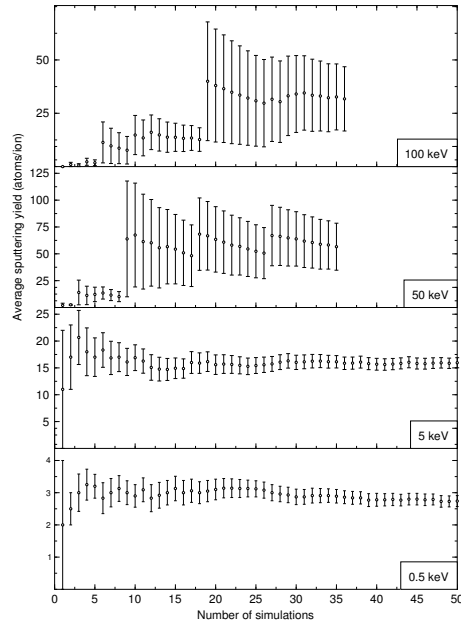


Fig. 1. Average sputtering yield as a function of the number of simulations. Results are from CEM potential simulations. The periodic pattern in the 50 and 100 keV series appears due to the stratified sampling of impact points. (See text.)

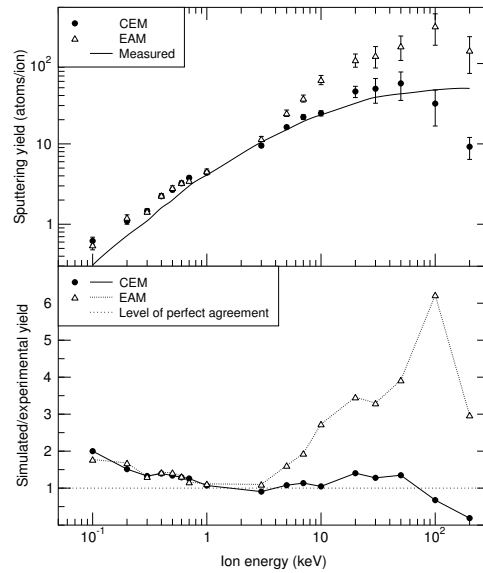


Fig. 2. Comparison of experimental and simulated sputtering yields of gold atoms from the Au(111) surface bombarded by Xe ions. Average yields (upper graph) are calculated from the simulation series in different energies. Errors are standard errors of the mean. Experimental values are from Ref. [24]. The lower graph shows the ratio between simulated and experimental yields.

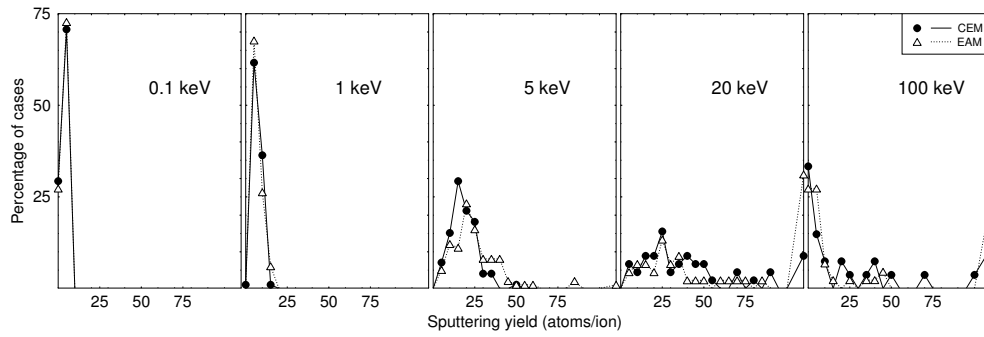


Fig. 3. Yield distributions at different energies.

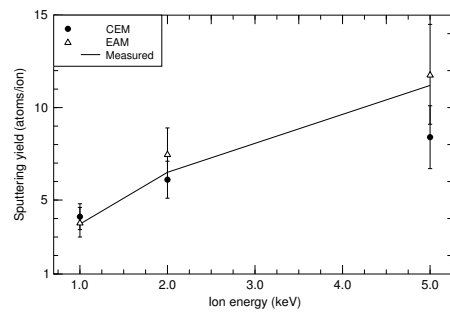


Fig. 4. Comparison of experimental and simulated average sputtering yields of gold atoms from the Au(111) surface bombarded by Ar ions. The experimental values are from Ref. [73,74]

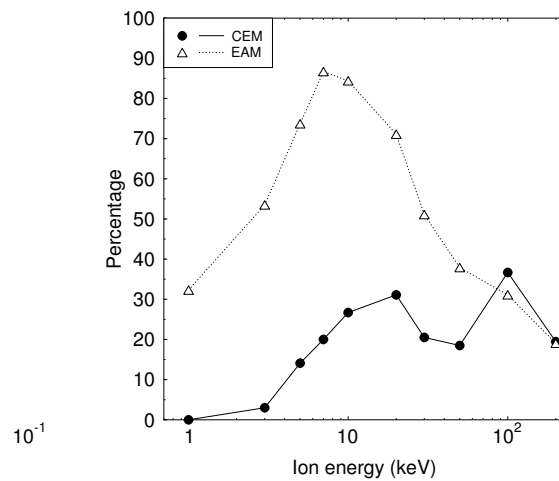


Fig. 5. Percentage of crater events out of all simulated events at different ion energies. The results are based on analysis of crater volumes and confirmed by visual inspection of simulations.

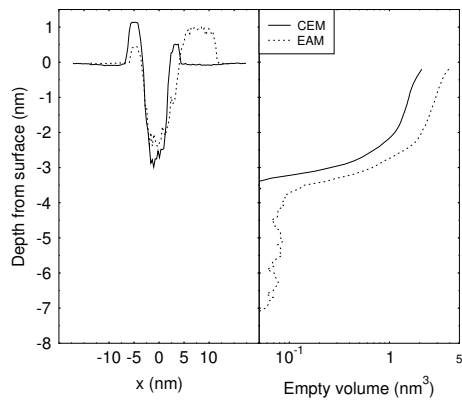


Fig. 6. Examples of crater profiles and the corresponding empty volume profiles of typical high yield events (50 keV, yield 278 atoms in the CEM event and 410 in the EAM event). The crater profiles illustrate crater shapes, whereas the empty volume profiles show the amount of empty space and vacancies as function of depth.

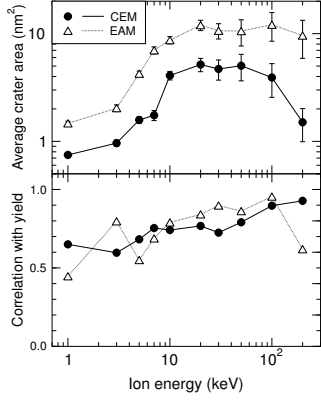


Fig. 7. Average crater areas (nm^2) and correlations between crater areas and sputtering yields at ion energies 1-200 keV. Crater areas are measured 0.3 nm below the lattice surface to prevent the depressions of one atom layer or less to contribute in the average. In figures 1-12 the lower panel shows the correlation between the quantity of upper panel and sputtering yield.

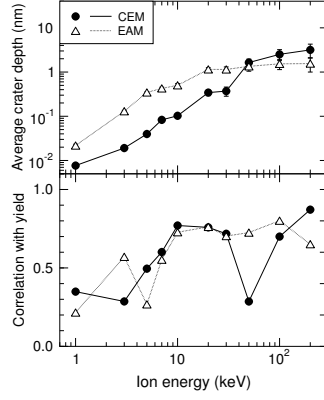


Fig. 8. Average crater depths (nm) and correlations between crater depths and sputtering yields at ion energies 1-200 keV. Only craters deeper than 0.2 nm are included in the averages.

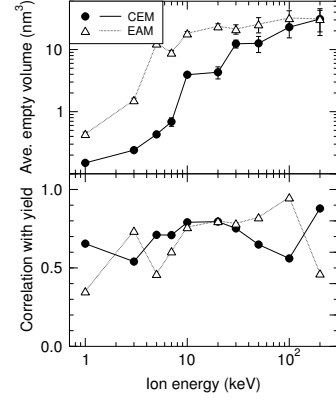


Fig. 9. Average empty volumes (nm^3) and correlations between empty volumes and sputtering yields at ion energies 1-200 keV. The empty volume consists of crater volume and total volume of vacancies near and below the crater. Volumes at 100 keV and 200 keV are too small and not strictly comparable to the volumes at the lower energies, because the whole ion energy is not deposited into the simulation cell in many events due to technical size limitations of simulation cells at these energies.

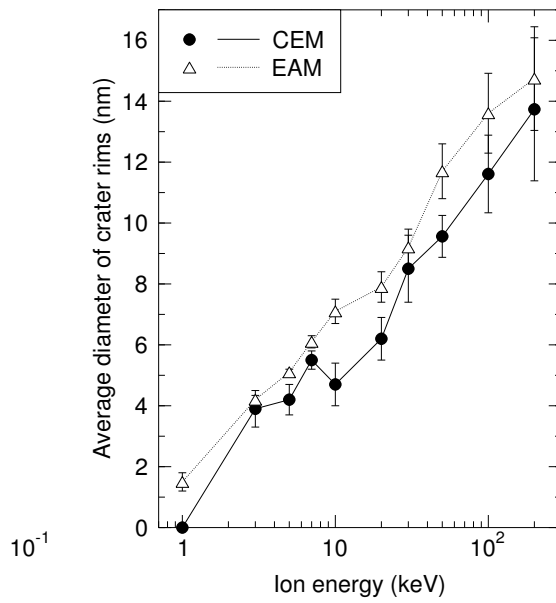


Fig. 10. Average maximum diameter of crater rims as a function of ion energy. Only clearly visible craters are included in the averages.

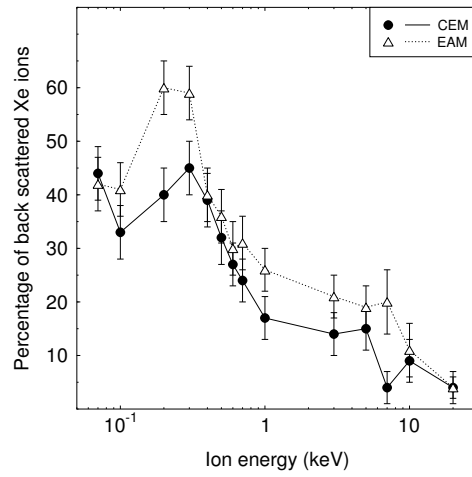


Fig. 11. Percentage of events where the Xe ion has scattered back from the lattice.

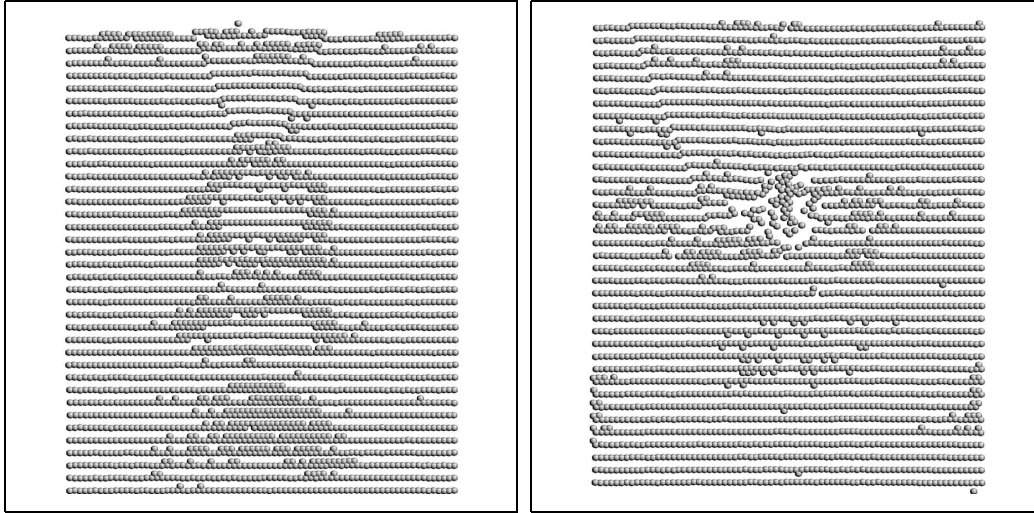


Fig. 12. Examples of defects caused by ion impacts into Au lattice showing the qualitative difference in crater formation between potentials. 50 keV Xe ion has come down from top and energy deposition has occurred in the area shown. A tetrahedral coherent displacement of atoms is clearly visible in the CEM event (left). The EAM event (right) has more irregular vacancy distribution, which is also true more generally. The slices of simulation lattices shown in the pictures are 20×27 nm wide and one Å thick, that is, only one atom layer with its defects is visible.